Acta Geotechnica (2012) 7:261–269
DOI 10.1007/s11440-012-0175-6

RESEARCH PAPER

Multiphysics hillslope processes triggering landslides

Ronaldo I. Borja · Xiaoyu Liu · Joshua A. White

Received: 21 December 2011 / Accepted: 20 April 2012 / Published online: 23 May 2012

Abstract In 1996, a portion of a highly instrumented experimental catchment in the Oregon coast range failed as a large debris flow from heavy rain. For the first time, we quantify the 3-D multiphysical aspects that triggered this event, including the coupled sediment deformation-fluid flow processes responsible for mobilizing the slope failure. Our analysis is based on a hydromechanical continuum model that accounts for the loss of sediment strength due to increased saturation as well as the frictional drag exerted by the moving fluid. Our studies highlight the dominant role that bedrock topography and rainfall history played in defining the failure mechanism, as indicated by the location of the scarp zone that was accurately predicted by our 3-D continuum model.

Keywords Hillslopes · Landslides · Multiphysics · Slope stability · Unsaturated soil

1 Introduction

Rainfall-induced landslides and/or debris flows threaten lives and property worldwide. Like earthquakes, they occur with little or no warning, and even with a warning it often applies to very large areas. Examples of high-profile slope failures include the 0.22 m storm of January 4, 1982 that combined with approximately 0.6 m of pre-storm seasonal rainfall, triggering thousands of landslides in the central coast ranges of California. In the San Francisco Bay Area alone, this storm resulted in 24 fatalities and millions of dollars in property damage [9, 31]. In 1985, a 0.56 m rainfall within a 24-h period triggered debris flows in Mameyes, Puerto Rico, resulting in 129 deaths [16]. In 1987, a 0.18 m rainfall in <5 h triggered numerous shallow landslides and debris flows in Rio Limón, Venezuela, resulting in 210 deaths [29]. In 1999, heavy rainfall exceeding 0.9 m over a 3-day period, with daily values >the 1,000-year return period in Vargas, Venezuela [18], killed 10s of 1,000s due to numerous landslides and severe flooding [34]. And in 2006, heavy rainfall triggered massive landslides in Guinsaugon, Philippines, burying an elementary school along with approximately 246 students and seven teachers [17].

Despite decades of extensive slope stability model development, the fundamental controls defining the triggering mechanisms of slope failure driven by rainfall are still not well quantified. It is generally known that increased saturation weakens a slope by reducing the capillary pressure holding the sediment particles together. It is also well-known that fluid flow enhances downhill slope movement by exerting frictional drag on the sediment. However, these are qualitative descriptions that do not help much in determining when a given slope will fail under what intensity of rainfall, and at what location will failure initiate if the slope indeed does fail. It is evident that the relevant processes are multiphysical in nature, involving both mechanical and hydrological processes. It is also evident that slope failure is influenced by the slope and bedrock topography, rainfall history, initial and boundary conditions, and the hydromechanical properties of the sediment. Assuming all of these parameters can be constrained, a question arises as to whether there exists a

R. I. Borja (✉) · X. Liu
Department of Civil and Environmental Engineering, Stanford University, Stanford, CA 94305, USA
e-mail: borja@stanford.edu

J. A. White
Computational Geosciences Group, Lawrence Livermore National Laboratory, Livermore, CA 94551, USA

model or a simulation tool that is accurate enough to make scientific predictions of the timing and location of slope failure. Demonstrating the accuracy of a model requires that it be validated against full-scale slopes that are known to have failed from a given rainfall.

In 1996, a portion of a highly instrumented experimental catchment in the Oregon coast range, known as the CB1 catchment, failed as a large debris flow after a period of intense rain. The slope movement at CB1 likely began as a landslide and eventually transformed into a debris flow as it left a distinct scarp zone on the uphill side delimiting the extent of the failure zone (Fig. 1). The location of this scarp zone is very important since it defines the boundary between the stable and mobilized regions in the slope. However, because the mobilized sediment flowed downwards and disturbed all the materials along its path, the extent of the debris flow zone on the downhill side simply delineates the runout distance of the sediment [21] but not the intrinsic lack of stability of the region during the initial flow mobilization. For this reason, we shall focus on the location of the upper scarp zone to infer the initial flow mobilization. CB1 had an extensive instrumentation program that provided one of the most comprehensive hydrologic response data sets for a steep, deforested catchment that experienced slope failure, and was an ideal field laboratory for validating a slope model.

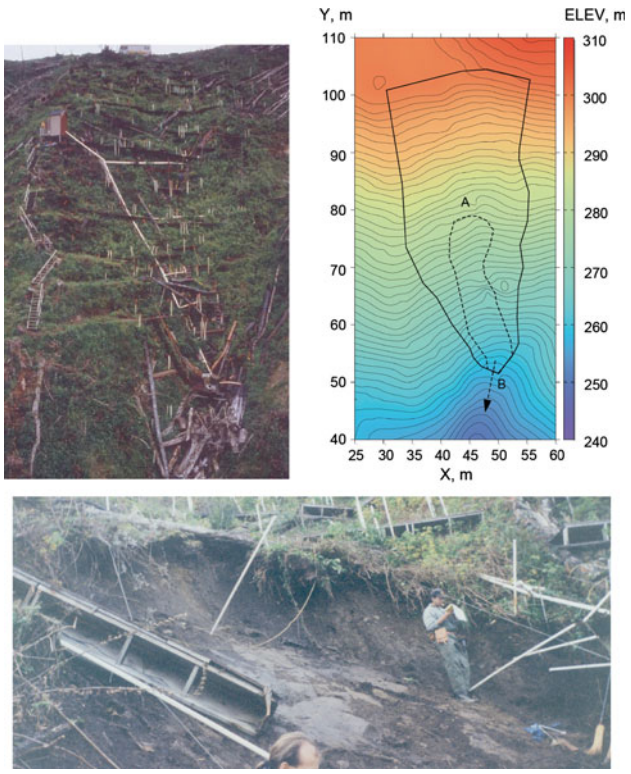

Fig. 1 The CB1 catchment. *Top left* slope face showing instrumentation; *top right* topographic map showing boundary of CB1 hydrologic instrumentation (*solid outline*) and debris flow zone (*dashed outline*), with *a* scarp zone, *b upper* weir position (*lower* weir is not mapped), and *arrow lower* debris flow trajectory; *bottom* image of scarp zone

In this paper, we show that it is possible to accurately identify hotspots for slope failure initiation using hydromechanical continuum modeling with CB1 as a case study. The slope model satisfies the relevant conservation laws, including the balance of momentum and balance of mass, as well as the governing constitutive laws for sediment deformation and fluid flow. The parameters of the model have been constrained from measurements conducted at the CB1 site as well as from tests of soil samples conducted in the laboratory. New to this paper is a full 3-D treatment of the slope, allowing us to assess the accuracy and limitations of the simplified 2-D representation of the problem [6, 8]. Results of this study have significant implications for an accurate prediction of the location of shallow landslides triggered by rainfall. As an aside, we remark that shallow landslides typically occur when a high-permeability soil is supported underneath by a low-permeability material (such as a bedrock), which traps the groundwater in the overlying soil and causes it to fail. Rainfall-triggered shallow landslides are a frequent occurrence on many hillslopes in Washington and Oregon [3, 11, 15, 20, 24], making this study extremely useful for understanding hillslope processes in those and similar regions. We do, however, limit the scope of this paper to the triggering of the slope failure only. Simulations of the mobilization and eventual deposition of the failed sediment [21, 32] are not included in this work.

2 The CB1 experimental catchment

The CB1 experimental catchment, clear-cut in 1987, is located along Mettman Ridge approximately 15 km north of Coos Bay in the Oregon Coast Range [12, 13]. CB1 is a 51-m-long (860 m^2) unchanneled valley with a north-facing aspect and an average slope of 43° (see Figure 1). Three sprinkling experiments were conducted at CB1: experiment #1 conducted in May 1990 at 1.5 mm/h for 6 days, experiment #2 conducted in May 1990 at 3.0 mm/h for 4 days, and experiment #3 conducted in May 1992 at 1.7 mm/h for 7 days. The instrumentation at CB1 characterized the spatial and temporal variability in near-surface hydrologic response for the three experiments and included an exhaustive grid of rain gauges, piezometers, tensiometers, TDR waveguide pairs (for estimating soil-water content), lysimeters, meteorological sensors (on a tower), atmometers, and weirs. Continuous measurements from rainfall, discharge, and total head (from selected piezometers) are available from 1990 through 1996. In November 1996 the CB1 slope failed as a large debris flow, leaving behind one of the most comprehensive hydrological

response data sets in existence for a steep, deforested catchment that has experienced slope failure. Figure 1 shows the extent of the debris flow zone resulting from the 1996 event.

The sediment at CB1 is colluvium, a surficial sediment derived from weathered or fresh bedrock, and the soil has no input from eolian transport. The parent rock for the colluvium is an Eocene turbidite sandstone from the Tyee and Flournoy formations. The soils are well mixed, non-plastic (plasticity index of zero), gravelly sands. The geometry and thickness of the colluvium are well defined from soil borings, which were used to generate the slope shown in Fig. 1 (the variation of colluvium thickness is not shown in this figure). Saturated hydraulic conductivity was determined from slug tests, soil-water content, and porosity from TDR measurements, and hysteretic capillary pressure relationships were also established. Studies from the discharge chemistry data indicate that runoff generation occurs primarily from water stored in small, unconnected pores and fractures in the bedrock and saprolite connecting with larger macropores during storms. The tracer data (bromide and isotopically-tagged water) suggest that the two most important flow paths at CB1 are rapid saturated flow through the shallow, fractured bedrock and vertical percolation in the vadose zone [1, 2]. The soil in the catchment is so conductive (saturated hydraulic conductivity $K_{\text{sat}} \approx 0.1$ cm/s) that neither is Horton overland flow produced nor does the phreatic surface typically reach the slope face during rain storms [1]. The tensiometer data indicate that the flux of water through the unsaturated zone provides a significant control on pore pressure development. Low confining stress triaxial shear tests demonstrate that the colluvium at CB1 is cohesionless (consisting of a sandy matrix); however, lateral root cohesion in clear-cut forests in the Oregon Coast Range is a source of apparent soil cohesion.

3 Mechanistic underpinnings

The conservation of groundwater mass in an unsaturated soil is described by the Richards equation [22]. However, this equation does not account for soil deformation. Ignoring the compressibility of water, we can rewrite this equation to include the solid deformation as [4, 5, 30]

$$\frac{\mathrm{d}\phi^{\mathrm{w}}}{\mathrm{d}t} + \phi^{w}\frac{\partial v_i}{\partial x_i} + \frac{\partial q_i^{w}}{\partial x_i} = \pm\theta^{b} \pm \theta^{e}, \tag{1}$$

where ϕ^{w} is the water volume fraction, v_i is the velocity of the solid matrix in the coordinate direction x_i, $q_i^{w} = \phi^{w}(v_i^{w} - v_i)$ is the relative discharge velocity, v_i^{w} and v_i are the velocity of water and solid in the direction x_i, θ^{b} is the specified rate source/sink, and θ^{e} is the rate of water exchange with the surface continuum. The deformation of the solid appears in the above equation through the velocity v_i.

An additional conservation law, the balance of linear momentum for the soil mass, must be enforced. To this end, we ignore inertia terms and write

$$\frac{\partial \sigma_{ij}}{\partial x_i} + \rho g_j = 0, \tag{2}$$

where σ_{ij} is the total Cauchy stress tensor, ρ is the total mass density of the sediment, and g_j is jth component of the gravity acceleration vector. An important step in the theoretical development is the decomposition of the total stress tensor σ_{ij} into an effective Cauchy stress tensor σ'_{ij} and a pore water pressure p [5],

$$\sigma_{ij} = \sigma'_{ij} - S_r p \delta_{ij}, \tag{3}$$

where S_r is the degree of saturation and δ_{ij} is the Kronecker delta. In the above equation, we assume that the pore air pressure remains equal to the atmospheric value, which is valid at shallow depths.

The constitutive equation for unsaturated flow is given by the generalized Darcy's law relating the relative water discharge velocity q_i with the hydraulic gradient,

$$q_i = -k_{rw} K_{\text{sat}} \frac{\partial}{\partial x_i}\left(\frac{p}{\rho_w \mathrm{g}} + z\right), \tag{4}$$

where K_{sat} is the hydraulic conductivity at complete saturation, k_{rw} is the relative permeability that varies with degree of saturation, g is the gravity acceleration constant, and z is the vertical coordinate. The constitutive equation for solid deformation relates the effective Cauchy stress rate $\dot{\sigma}'_{ij}$ with the sediment strain rate $\dot{\epsilon}_{kl}$ through the tangent stress-strain tensor c_{ijkl} as

$$\dot{\sigma}'_{ij} = c_{ijkl}\dot{\epsilon}_{kl}. \tag{5}$$

The tangent stress–strain tensor c_{ijkl} depends on the specific constitutive model for the sediment, and here we employ an elastic perfectly plastic Drucker–Prager model for the colluvium. This plasticity model is appropriate for modeling the behavior or soils, rocks, and other cohesive-frictional materials [7].

In the unsaturated zone, a characteristic curve exists between the degree of saturation S_r and the capillary stress $-p > 0$. This curve exhibits hysteresis with distinct drying and wetting branches [14]. In general, the stability of a slope may be influenced by both the wetting and drying branches of the water retention curve. However, for the present study, rainfall infiltration increases the degree of saturation and activates the wetting branch of the curve, which is expressed for the colluvium by the Van Genuchten [35] equation as

$$S_r[\%] = 32 + 68/\left[1 + \left(\frac{-p}{0.40}\right)^3\right]^{2/3}, \quad (6)$$

where $p < 0$ is given in kPa. The relative permeability k_{rw} for the colluvium has a similar exponential form

$$k_{rw}(\theta) = \theta^{1/2}\left[1 - \left(1 - \theta^{3/2}\right)^{2/3}\right]^2, \quad \theta = \frac{S_r[\%] - 32}{68}. \quad (7)$$

Ebel et al. [12, 13] and Torres et al. [33] compiled experimental data leading to the above hydrologic coefficients. The specific values of the hydrologic coefficients are the same as those summarized in Refs. [6, 8].

Because of the nonlinear nature of the partial differential equations and the complex geometry of the slope, a numerical approximation is needed, and here we use the finite element method. Figure 2 shows two finite element meshes used in this study. They were derived from slope and bedrock topographies obtained from detailed theodolite surveys and piezometer installations by Montgomery et al. [19]. The more permeable colluvium layer is on the order of 1 meter thick underlain by a bedrock. Because the bedrock is significantly stronger and stiffer than the sediment, it is not included in the deformation model; however, it can act as a fluid source or sink because of the high-density fractures. The sediment is modeled using eight-node "mixed" hexahedral elements where each node has three displacement and one pore pressure degrees of freedom. These elements facilitate a simultaneous solution of the coupled fluid flow/solid deformation problem and have been numerically stabilized to ensure that they behave well for incompressible applications [36]. For long-duration simulations with a large number of time steps, we used the coarser mesh. For short-duration simulations involving hypothetical rainfall scenarios, we used both meshes and compared the results. As noted later in this paper, the coarser mesh captures the essential features of the solution quite well and is thus suitable for the more computationally intensive long-duration simulations.

The colluvium at CB1 is a sandy matrix with a friction angle ranging from 35 to 44° [10, 25–28, 37, 38]. Lateral root cohesion in clear-cut forests in the Oregon Coast Range was estimated to be uniformly <10 kPa [27] and may have explained how such a steep slope at CB1 had been sustained by the sediment for such a long time. For purposes of analysis, baseline values of 40° for the friction angle, 4 kPa for cohesion, and 25° for dilatancy angle have been used in the simulations. Sensitivity studies to perturbations in these material parameters have been presented in Ref. [6] to better understand how the results would be influenced by their values. The saturated density of the soil is about 1,600 kg/cu m [27], and the bulk density at soil water contents of 20–30 % is around 1,200 kg/cu m [26].

4 Simulations and results

Figure 3 depicts the hyetograph preceding the initial flow mobilization. Despite the highly erratic variation of rainfall, it is evident from this figure that the intense storm of November 19 was the trigger to the slope failure at CB1. The graph indicates on-and-off precipitation for several days preceding the peak rain. For purposes of simulation, we prescribed a simplified rain consisting of a flux of 6 mm/h for 24 h followed by a flux of 40 mm/h for 1.7 h on the slope face (cf. Fig. 3). As noted earlier, the soil is so conductive that Horton overland flow could hardly be produced during storms, so we assumed that all of the

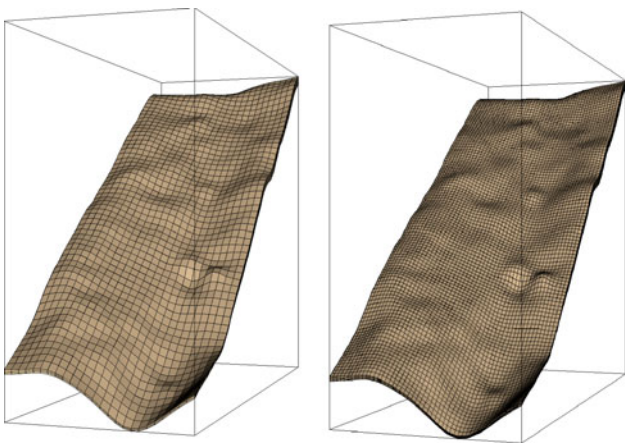

Fig. 2 Finite element meshes for multiphysical analyses of CB1 slope failure: coarser mesh with 4.5K elements, 6.4K nodes, and 25.4K degrees of freedom (*left*); and finer mesh with 36 K elements, 43.2K nodes, and 173K degrees of freedom (*right*)

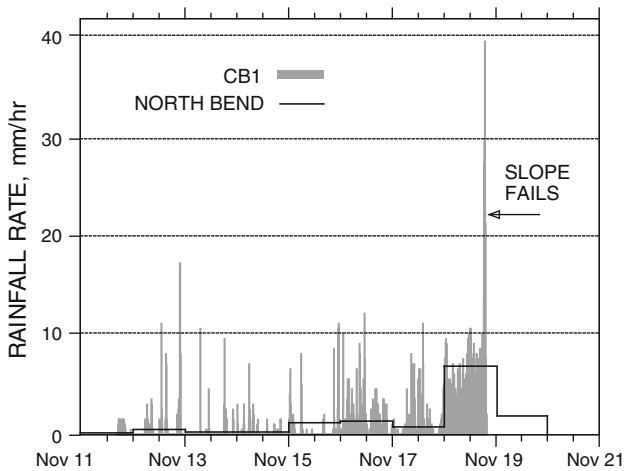

Fig. 3 Hyetograph triggering debris flow at the CB1 catchment, superimposed with hyetograph at nearby North Bend airport

fluxes on the slope face percolated into the soil. The simplified rain sequence produced approximately the same volume of water over the time interval of actual rain and also captured the short-duration intense rain that triggered the slope failure at CB1. Fluid input from the bedrock fractures is one of the main sources of uncertainty and has been neglected in the first set of simulations. It must be noted that assuming an impermeable bedrock is conservative if in fact the fractures can absorb rainwater from the top soil. However, if the bedrock fractures are a source of fluid, then the location of the fractures and the quantity of fluid input from them could potentially impact the pattern and timing of slope failure [6, 8]. To investigate this aspect, we conducted a second set of simulations incorporating fluid input from the bedrock and assessed its effect on slope failure initiation.

At the beginning of the simulation assuming an impermeable bedrock, which we denote as Case A, a uniform initial pressure of -1.5 kPa was prescribed in the soil representing an approximate initial saturation condition in the colluvium. This is a relatively low suction stress [23] reflecting the effects of on-and-off precipitation for several days prior to the peak rain. While this may be considered a gross simplification, previous studies [6, 8] suggest that the colluvium would have to be fully saturated for the slope to fail. To model the rainfall event, a time-dependent fluid flux q on the ground surface was applied continually until a seepage face condition was detected, at which point, the boundary condition was switched to a fixed pressure $p = 0$. In this sequence, a prescribed flux is a natural boundary condition, whereas a prescribed pressure is an essential boundary condition. Formation of a seepage face thus entails switching the boundary condition type on the slope face from natural to essential.

Figure 4 shows the spatial distribution of plastic strain on the sediment layer in contact with the bedrock at the end of the intense rain sequence. The elastic strains are typically much smaller than the plastic strains, so the plastic strain contour may be taken as a measure of the total distortion of the sediment in contact with the bedrock. The plastic strain plotted in this figure is the second invariant of the deviatoric component of the full plastic strain tensor, which has six independent components in 3-D, and is a scalar measure of overall plastic distortion. Using this plastic strain as a variable to identify hotspots for slope failure, the model remarkably predicted the scarp zone at CB1 with good accuracy. The pore water pressure distribution shows positive values on the colluvium–bedrock interface, suggesting that the bottom of the colluvium has reached full saturation almost everywhere on this interface. However, the highest pore water pressure concentrates within the zone of intense plastic strain, indicating that the pore pressure buildup is the driving force behind the

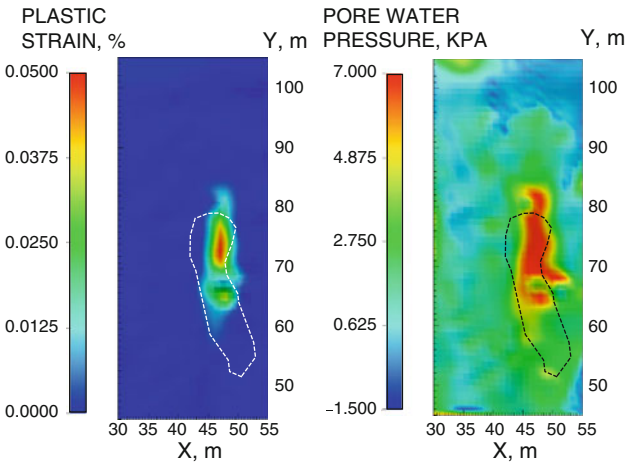

Fig. 4 Case A: equivalent plastic strain (*left*) and pore water pressure (*right*) on colluvium–bedrock interface after prescribing a rainfall of 6 mm/h for 24 h followed by 40 mm/h for 1.7 h with an impermeable bedrock. *Dashed curve* is extent of debris flow zone in CB1

localized deformation. The pore pressures are high enough for the fully saturated zone to reach the slope face, suggesting that a significant seepage face area has formed during this rain sequence.

Indeed, Fig. 5 reveals that a significant portion of the slope face has transitioned into a seepage face (red zone in the pore pressure contour). In contrast, the plastic strain contour is limited to a much smaller region, concentrated mainly in areas where locally steep slopes rapidly flatten out into horizontal steps. A steep slope enhances high-velocity fluid flow, but where it meets a step, the fluid flow slows down, resulting in a local accumulation of groundwater. This could explain the local buildup of high fluid pressures in this region of the CB1 catchment (Fig. 4). Therefore, irregular slope geometry could have combined with rainfall history to trigger localized deformation in the CB1 catchment.

Quantifying the fluid input from the bedrock fractures in CB1 requires a deep understanding of the subsurface flow

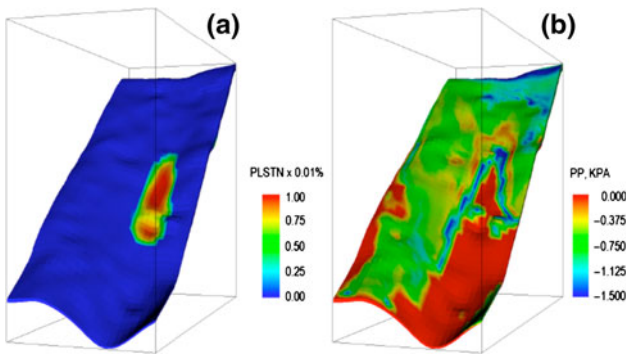

Fig. 5 Case A: equivalent plastic strain (*left*) and pore water pressure (*right*) on the slope face after prescribing a rainfall of 6 mm/h for 24 h followed by 40 mm/h for 1.7 h

paths in this steep unchanneled catchment. As noted earlier, tracer studies [2] revealed two important flow paths through the catchment: vertical percolation in the vadose zone and rapid saturated flow in the colluvium. Flow paths meet in a small area of the colluvium near the upper weir B shown in Fig. 1. Tracer data also revealed that it is in the latter zone where predominantly fresh rain water from the colluvium mixes with high-velocity but long residence time water emerging from the bedrock. The dynamics of this zone dictate the resulting runoff chemistry in general, and the proportions of old and new water in runoff in particular [2].

It is not possible to distinguish between release of old stored water and flow of new water as sources of runoff during actual winter storms. Fortunately, the hydromechanical model used in this study does not distinguish between the two sources of runoff. In calculating slope deformations, what matters is the current fluid gradient resulting from the imposed fluid fluxes on the colluvium boundary, and not the material origin of the runoff. Thus, we simultaneously prescribed natural rainfall on the slope face and fluid input from the bedrock, the latter resembling a "reverse rain," to assess the effect of bedrock fracture flows on slope deformation. For Case B, a reverse rain equal to 10 % of the slope rain was prescribed over the entire colluvium–bedrock interface, mimicking a bedrock of uniform fracture density. For Case C, a reverse rain having the same intensity as the slope rain but with a time lag of 10 min was prescribed over a 6-m area on the uphill side of the top weir, mimicking the results of the tracer studies. The intent of these additional simulations was not to capture the actual fluid input from the bedrock, which is unknown, but rather, to simply get a feel for how these additional boundary conditions would impact the mechanism of slope deformation.

Results of the simulations for Cases B and C are shown in Figs. 6 and 7 respectively. As expected, the bedrock fluid input slightly enlarged the zones of saturation and plastic strain, although the mechanism of deformation and critical zones remain essentially the same as those predicted by the simulation with an impermeable bedrock (Fig. 4). While it may look like the bedrock fluid had little effect on slope deformation, it is possible that it could have contributed to slope failure in other ways. For example, it could have caused a decrease in the value of the contact friction angle between the colluvium and bedrock causing the sediment to slide, or it could have induced the plant roots to pull out from the soil causing the effective cohesion to disappear. However, any simulation of these effects would be conjectural since there are no concrete data supporting such mechanisms. What seems evident from the simulations, however, was that the combined effects of local topography and rainfall history were dominant

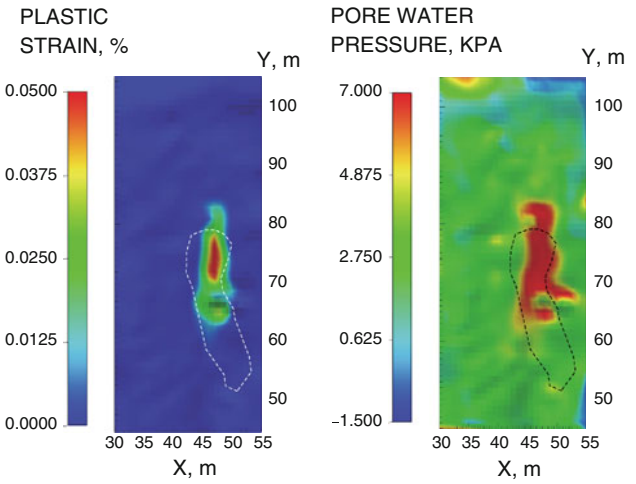

Fig. 6 Case B: equivalent plastic strain (*left*) and pore water pressure (*right*) on colluvium–bedrock interface after prescribing a slope rain of 6 mm/h for 24 h followed by 40 mm/h for 1.7 h, combined with a reverse rain of 0.6 mm/h for 24 h followed by 4 mm/h for 1.7 h. *Dashed curve* is extent of debris flow zone at CB1

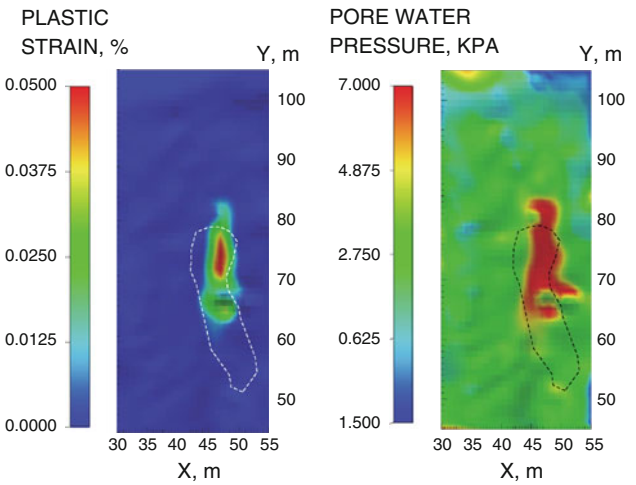

Fig. 7 Case C: equivalent plastic strain (*left*) and pore water pressure (*right*) on colluvium–bedrock interface after prescribing a rainfall of 6 mm/h for 24 h followed by 40 mm/h for 1.7 h, combined with the same time–history reverse rain with a time lag of 10 min over a 6-m area *above* the *top* weir. *Dashed curve* is extent of debris flow zone at CB1

enough to explain the mechanisms of slope failure in the CB1 catchment, with or without fluid input from the bedrock. If we had oversimplified the slope and bedrock topography and/or drastically changed the rainfall history, previous studies [8] revealed that we would have arrived at a completely different failure mechanism that is inconsistent with that observed in the catchment. This indicates the potential of high-fidelity multiphysical simulations for capturing the relevant field processes at the catchment scale.

5 Mesh sensitivity, rainfall history, and 3-D effects

In a recent article [8], the authors used a plane strain representation of the CB1 problem to infer the factor of safety for this slope from hydromechanical continuum modeling. The results of their studies highlighted the important role that the pore pressure played in triggering slope failure, as well as demonstrated a remarkable agreement between the continuum hydromechanical and limit equilibrium solutions in predicting the relevant failure mechanisms. Unfortunately, the following results also reveal the inherent deficiencies of a 2-D representation of what is truly a 3-D problem.

We consider a short-duration rainfall of 50 mm/h for 2.5 h applied on the slope face, beginning with the same initial pore pressure of −1.5 kPa in the colluvium and assuming the bedrock to be impermeable. Figure 8 shows the plastic strain contours on the colluvium–bedrock interface generated by this rainfall using the coarser and finer meshes shown in Fig. 2. We see that the finer mesh produced a slightly softer deformation response and resolved the details of deformation more accurately, which is to be expected. However, the coarser mesh captured the essential mechanism of deformation nearly as accurately. In particular, both meshes identified the same hotspots for deformation with the most intense plastic strain as being the zone located approximately 15 m *below* the actual scarp zone, suggesting a different dominant failure mechanism than the one predicted in the previous section with a different rainfall history. This suggests that rainfall history does have a significant impact on the resulting deformation and failure mechanisms for this slope.

With the same hypothetical rainfall under plane strain condition on the plane defined by the dashed straight lines in Fig. 8, the authors [8] predicted the scarp zone to develop at a point located approximately 10 m *above* the actual scarp zone, labeled as a white star in Fig. 8. This same white star was labeled as inflection point C3 in the plane strain model of Ref. [8]. We should note that limit equilibrium solutions derived from the same pore pressure distribution on the colluvium–bedrock interface predicted the same scarp zone, namely, at inflection point C3. Clearly, this result is not in agreement with the calculated 3-D deformation, which shows very faint plastic yielding at this zone. Therefore, the kinematical constraints imposed by the plane strain assumption (including the planar fluid flow pattern) changed the mechanism of deformation and resulted in the prediction of a different failure mechanism.

In summary, the results of Fig. 8 suggest the following: (a) the coarser mesh is sufficient for identifying the primary pattern of deformation and mechanism of slope failure; (b) rainfall history has an important effect on the mechanism of deformation and slope failure; and (c) a 2-D representation may not be sufficient to fully characterize the pattern of deformation and failure on a slope that has strong 3-D features.

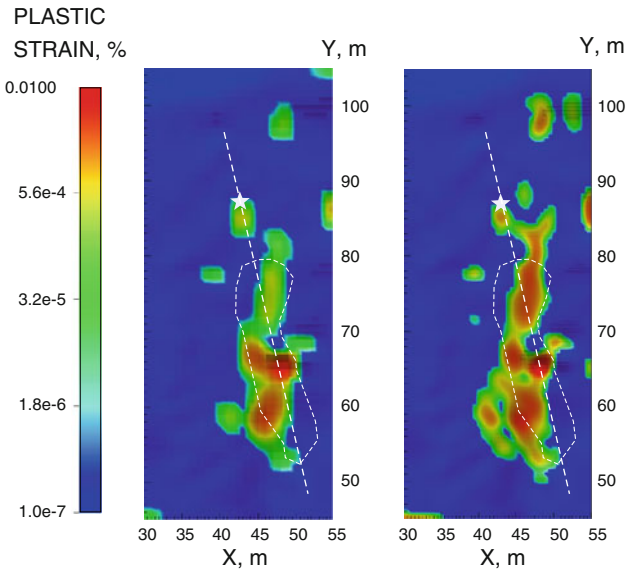

Fig. 8 Mesh sensitivity study: equivalent plastic strain on colluvium–bedrock interface after prescribing a rainfall of 50 mm/h for 2.5 h with an impermeable bedrock: coarser mesh (*left*) and finer mesh (*right*). *Dashed curve* is extent of debris flow zone in CB1; *white star* is inflection point C3 identified as the primary scarp zone in the plane strain model of Ref. [8]

6 Closure

A 3-D hydromechanical model was developed to investigate a rainfall-induced slope failure at a highly instrumented experimental catchment near the Oregon Coast Range. The model accounts for the loss of sediment shear strength due to increased saturation and the coupled solid deformation-fluid flow processes expected in a slope subjected to intense rainfall infiltration. The model accurately predicted the mechanism of slope failure in the catchment, specifically, the location of the scarp zone, suggesting the potential of 3-D hydromechanical modeling for investigating more general hillslope scenarios. As for the specific catchment investigated in this paper, numerical simulations suggest that the slope failure was triggered by the local topography and rainfall history at the site, while fluid flow through the fractures of the bedrock did not appear to be dominant enough to alter the mechanism of slope failure. However, since failure is an instability problem that is sensitive to small variations of the load, fluid flow through the bedrock fractures could have enhanced the deformation as manifested by the enlarged zone of plastic strain.

Acknowledgments The authors are grateful to Drs. Keith Loague and Brian Ebel for numerous discussions pertaining to the CB1

catchment, and to the three anonymous reviewers for their constructive reviews. This work was supported by the US National Science Foundation (NSF) under Contract Numbers CMMI-0824440 and CMMI-0936421 to Stanford University.

References

1. Anderson SP, Dietrich WE, Torres R, Montgomery DR, Loague K (1997) Concentration–discharge relationships in runoff from a steep, unchanneled catchment. Water Resour Res 33:211–225
2. Anderson SP, Dietrich WE, Montgomery DR, Torres R, Conrad ME, Loague K (1997) Subsurface flow paths in a steep, unchanneled catchment. Water Resour Res 33:2637–2653
3. Baum RL, Harp EL, Hultman WA (2000) Map showing recent and historic landslide activity on coastal bluffs of Puget Sound between Shilshole Bay and Everett, Washington. U.S. Geological Survey Miscellaneous Field Studies Map MF-2346. http://pubs.usgs.gov/mf/2000/mf-2346/
4. Borja RI (2004) Cam–clay plasticity, part V: a mathematical framework for three-phase deformation and strain localization analyses of partially saturated porous media. Comput Method Appl Mech Eng 193:5301–5338
5. Borja RI (2006) On the mechanical energy and effective stress in saturated and unsaturated porous continua. Int J Solids Struct 43:1764–1786
6. Borja RI, White JA (2010) Continuum deformation and stability analyses of a steep hillside slope under rainfall infiltration. Acta Geotech 5:1–14
7. Borja RI (2012) Plasticity modeling and computation. Springer, Heidelberg (in press)
8. Borja RI, White JA, Liu X, Wu W (2012) Factor of safety in a partially saturated slope inferred from hydro-mechanical continuum modeling. Int J Numer Anal Method Geomech 36:236–248
9. Brown WM III, Sitar N, Saarinen TF, Blair ML (1984) Debris flows, landslides, and floods in the San Francisco Bay region, January 1982. Overview of and summary of a conference held at Stanford University, August 23–26, 1982, Washington DC, National Research Council and USGS, p 83
10. Burroughs ER Jr, Hammond CJ, Booth GD (1985) Relative stability estimation for potential debris avalanche sites using field data. In: Proceedings of the international symposium on erosion, debris flow and disaster prevention, Tsukuba, Japan, pp 335–339
11. Coe JA, Michael JA, Crovelli RA, Savage WZ, Laprade WT, Nashem WD (2004) Probabilistic assessment of precipitation-triggered landslides using historical records of landslides occurrence, Seattle,Washington. Environ Eng Geosc 10:103–112
12. Ebel BA, Loague K, Dietrich WE, Montgomery DR, Torres R, Anderson SP, Giambelluca TW (2007) Near-surface hydrologic response for a steep, unchanneled catchment near Coos Bay, Oregon: 1. Sprinkling experiments. Am J Sci 307:678–708
13. Ebel BA, Loague K, VanderKwaak JE, Dietrich WE, Montgomery DR, Torres R, Anderson SP (2007) Near-surface hydrologic response for a steep, unchanneled catchment near Coos Bay, Oregon: 2. Physics-based simulations. Am J Sci 307:709–748
14. Ebel BA, Loague K, Borja RI (2010) The impacts of hysteresis on variably saturated hydrologic response and slope failure. Environ Earth Sci 61:1215–1225
15. Godt JW (2004) Observed and modeled rainfall conditions for shallow landsliding in the Seattle,Washington, area, Ph.D. thesis, University of Colorado, p 151
16. Jibson RW (1992) The Mameyes, Puerto Rico, landslide disaster of October, 7, 1985. In: Slosson JE, Keene AG, Johnson JA (eds) Landslides/landslide mitigation, reviews in engineering geology. Geological Society of America, Boulder, CO, pp 37–54
17. Lagmay AMA, Ong JBT, Fernandez DFD, Lapus MR, Rodolfo RS, Tengonciang AMP, Soria JLA, Baliatan EG, Quimba ZL, Uichanco CL, Paguican EMR, Remedio ARC, Lorenzo GRH, Avila FB, Valdivia W (2006) Scientists investigate recent Philippine landslide. Eos Trans AGU 87(12):121
18. Martínez E (2002) Evento Meteorologico sobre el Litoral Central en Diciembre 1999. Informe Inédito
19. Montgomery DR, Dietrich WE, Torres R, Anderson SP, Heffner JT, Loague K (1997) Hydrologic response of a steep, unchanneled valley to natural and applied rainfall. Water Resour Res 33:91–109
20. Montgomery DR, Greenberg HM, Laprade WT, Nashem WD (2001) Sliding in Seattle: test of a model of shallow landsliding potential in an urban environment. In: Wigmosta MS, Burges SJ (eds) Land use and watersheds: human influence on hydrology and geomorphology in urban and forest areas—water science and application, American Geophyisical Union, Washington, DC, pp 59–73
21. Moriguchi S, Borja RI, Yashima A, Sawada K (2009) Estimating the impact force generated by granular flow on a rigid obstruction. Acta Geotech 4:57–71
22. Richards LA (1931) Capillary conduction of liquids in porous mediums. Physics 1:318–333
23. Salager S, Rizzi M, Laloui L (2011) An innovative device for determining the soil water retention curve under high suction at different temperatures. Acta Geotech 6:135–142
24. Salciarini D, Godt JW, Savage WZ, Baum RL, Conversini P (2008) Modeling landslide recurrence in Seattle, Washington, USA. Eng Geol 102:227–237
25. Schmidt KM (1994) Mountain scale strength properties, deep-seated landsliding and relief limits. MS thesis, Department of Geological Sciences, University of Washington, Seattle
26. Schmidt KM (1999) Root strength, colluvial soil depth, and colluvial transport on landslide-prone hillslopes. Ph.D. dissertation, Department of Geological Sciences, University of Washington, Seattle
27. Schmidt KM, Roering JJ, Stock JD, Dietrich WE, Montgomery DR, Schaub T (2001) The variability of root cohesion as an influence on shallow landslide susceptibility in the Oregon Coast Range. Can Geotech J 38:995–1024
28. Schroeder WL, Alto JV (1983) Soil properties for slope stability analysis; Oregon and Washington coastal mountains. For Sci 29:823–833
29. Schuster RL, Salcedo DA, Valenzuela L (2002) Overview of catastrophic landslides of South America in the twentieth century. In: Evans SG, DeGraff JV (eds) Catastrophic landslides: effects, occurrence, and mechanisms, reviews in engineering geology. Geological Society of America, Boulder, CO, pp 1–33
30. Sharma RJ, Konietzki H, Kosugi K (2010) Numerical analysis of soil pipe effects on hillslope water dynamics. Acta Geotech 5:33–42
31. Smith TC, Hart EW (1982) Landslides and related storm damage, January 1982, San Francisco Bay region. Calif Geol 35:139–152
32. Teufelsbauer H, Wang Y, Pudasaini SP, Borja RI, Wu W (2011) DEM simulation of impact force exerted by granular flow on rigid structures. Acta Geotech 6:119–133
33. Torres R, Dietrich WE, Montgomery DR, Anderson SP, Loague K (1998) Unsaturated zone processes and the hydrologic response of a steep, unchanneled catchment. Water Resour Res 34:1865–1879
34. USAID (2000) Venezuela factsheet, February, 2000. USAID-Office of Foreign Disaster Assistance, p 2
35. Van Genuchten MT (1980) A closed-form equation for predicting the hydraulic conductivity of unsaturated soils. Soil Sci Soc Am J 44:892–898

36. White JA, Borja RI (2008) Stabilized low-order finite elements for coupled solid-deformation/fluid-diffusion and their application to fault zone transients. Comput Method Appl Mech Eng 197:4353–4366
37. Wu TH, Beal PE, Lan C (1988) In-situ shear test of soil-root systems. J Geotech Eng ASCE 114:1376–1394
38. Yee CS, Harr DR (1977) Influence of soil aggregation on slope stability in the Oregon Coast Range. Environ Geol 1:367–377